COMPDYN 2013
4th ECCOMAS Thematic Conference on
Computational Methods in Structural Dynamics and Earthquake Engineering
M. Papadrakakis, V. Papadopoulos, V. Plevris (eds.)
Kos Island, Greece, 12–14 June 2013

UNCERTAINTY QUANTIFICATION OF THE NONLINEAR DYNAMICS OF ELECTROMECHANICAL COUPLED SYSTEMS

Roberta de Queiroz Lima[1,2] **and Rubens Sampaio**[1]

[1]Pontifícia Universidade Católica do Rio de Janeiro
Marquês de São Vicente, 225, Gávea, RJ, CEP: 22453-900, Brazil
e-mail: rsampaio@puc-rio.br

[2] Universit Paris-Est, Laboratoire Modlisation et Simulation Multi Echelle
MSME UMR 8208 CNRS, 5 bd Descartes, 77454 Marne-la-Valle, France
e-mail: roberta.dequeirozlima@univ-paris-est.fr

Keywords: Nonlinear dynamics, coupled systems, friction, stochastic analysis.

Abstract. *This paper analyzes the nonlinear stochastic dynamics of electromechanical systems with friction in the coupling mechanism and in the mechanical parts. Two different electromechanical systems were studied. The first one is composed by a cart whose motion is excited by a DC motor and in the second a new element,a pendulum, is attached to the cart. The suspension point of the pendulum is fixed in cart, so that exists a relative motion between them. The influence of the DC motor in the dynamic behavior of the system is considered. The coupling between the motor and the cart is made by a mechanism called scotch yoke, so that the motor rotational motion is transformed in horizontal cart motion over a rail. In the model of the system, it is considered the existence of friction in the coupling mechanism and in between the cart and the rail. The embarked pendulum is modeled as a mathematical pendulum (bar without mass and particle of mass m_p at the end). The embarked mass introduces a new feature in the system since the motion of the pendulum acts as a reservoir of energy, i.e. energy from the electrical system is pumped to the pendulum and stored in the pendulum motion, changing the characteristics of the mechanical system. Due to the consideration of friction, the dynamic of the problem is described by a system of differential algebraic equations. One of the most important parameters of the problem is the amplitude of the cart motion that is given by the position of the pin used in the coupling mechanism. The behavior of the system is very sensitive to this parameter because it controls the nonlinearities of the problem. In the stochastic analysis, this parameter is considered uncertain and is modeled as a random variable. The Maximum Entropy Principle is used to construct its probability model. Monte Carlo simulations are employed to compute the mean motion and the 90% confidence interval of the displacements of the pendulum, of the cart and of the angular speed of the motor shaft.*

1 INTRODUCTION

The wide occurrence of the electromechanical coupling in manufacturing processes turns the research on this topic an area of interest for engineering practice. By coupling it is meant a mutual influence between the systems. In the two systems studied in this paper the source of energy is the imposed voltage that will be taken as constant. The dynamics of the motor is heavily influenced by the coupled mechanical system. It is believed that the theoretical knowledge on couplings between electric motors and mechanical systems can provide improvements in the design of mechanical systems and can help in the development of control techniques.

Electromechanical coupled systems is not a new subject, in [1] there is a chapter dedicated to the coupled problem and it is remarked that it is a problem different from parametric resonance. In [2] the whole book is dedicated to the problem but the analytical treatment supposes some small parameter, a hypothesis avoided here. Recently, the problem is been intensely studied again, see [3, 4, 5], but the literature is vast. It is important to remark that the nonlinearity of this problem is not prescribed by a function, as is unfortunately found in several papers, but it comes from the coupling and the nonlinearity varies with the coupling conditions. This means that the no linearity varies with the dynamics, one cannot that it a sine, or a cubic nonlinearity, as seen in some papers, for example. Coupled problems have a very rich system dynamics due to presence of nonlinearities arising from the mutual interaction of the coupled systems, see [6, 7, 8, 9, 10].

In this paper, it is analyzed and compared two electromechanical systems. The first one is a very simple system composed by a cart whose motion is driven by a DC motor. The coupling between the motor and the cart is made by a mechanism called *scotch yoke*. In this simple system the coupling is a sort of master-slave condition: the motor drives, the cart is driven, and that is all. The second system has the same two elements of the first and also a pendulum that can move relative to the cart. The pendulum introduces a new feature since the motion of the pendulum acts as a reservoir of energy, i.e. energy from the electrical system is pumped to the pendulum and stored in the pendulum motion, changing the characteristics of the mechanical system. The pendulum is the embarked system and its motion is driven by the motion of the cart or, better said, by the motor. The motor is influenced by the attached mass and the heavier the mass the greater the nonlinearities involved. Normally, problems of this type are modeled saying that the forcing is harmonic with frequency given by the nominal frequency of the motor. It will be shown here that this hypothesis is far from true.

Without simplifying hypothesis about the terms, the behavior of the system variables are analyzed, as the motor current over time, rotational movement of the motor shaft and force and torque exerted by the DC motor in the mass. The influence of the pendulum embarked in the cart is investigated and it is shown the changes it causes in the dynamics of the second system with respect to the first.

To better see the effects of coupling, two different analysis are developed to the coupled systems. In the first one, it is considered that the mechanical system has no dissipation, the only dissipation is in the electrical part. In the second one, it is considered the existence of friction in the mechanical part.

The two most important parameters of the coupled problem are the attached mass and the amplitude of its motion that is given by the position of the pin used in the coupling. With some simplifying hypothesis a lot of analytical results could have been derived as well as results about chaotic behavior, but this is not the object of the paper. The object is to show the dynamics without undue simplifications.

This paper is organized as follows. Section 2 describes the two coupled electromechanical systems analyzed. Section 3 presents the results of the deterministic simulations developed to each one of them in the case of consideration and no consideration of friction. The influence of the attached mass and the amplitude of its motion are discussed. Also in Section 3, it is presented a configuration of the coupled system that leads to the phenomenon of energy pumping and causes revolution, i. e. the inversion of the master-slave relation. The probability model to the parameter that is considered uncertain is construct in Section 4 and the results of the simulations of the stochastic systems are presented in Section 5. Section 6 presents some conclusions.

2 DYNAMICS OF THE COUPLED SYSTEMS

Next, it is presented the elements of the two coupled systems (motor, cart, and pendulum). The coupling between the motor and the mechanical systems are shown and the two coupled problems are described and mathematically formulated as initial-value problems.

2.1 Electrical system: motor DC

The mathematical modeling of DC motors is based on the Kirchhoff's law [11]. It is constituted by the equations

$$l\dot{c}(t) + r\,c(t) + k_e\dot{\alpha}(t) = v\,, \tag{1}$$

$$j_m\ddot{\alpha}(t) + b_m\dot{\alpha}(t) - k_t\,c(t) = -\tau(t)\,, \tag{2}$$

where t is the time, v is the source voltage, c is the electric current, $\dot{\alpha}$ is the angular speed of the motor, l is the electric inductance, j_m is the motor moment of inertia, b_m is the damping ratio in the transmission of the torque generated by the motor to drive the coupled mechanical system, k_t is the torque constant, k_e is the motor electromagnetic force constant and r is the electrical resistance. Figure 1 shows a sketch of a DC motor. The available torque to the coupled mechanical system is represented by τ, that is the component of the torque vector $\vec{\tau}$ in the z direction shown in Fig. 1.

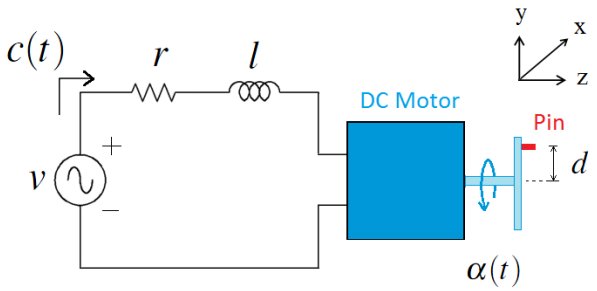

Figure 1: Electrical motor DC.

Assuming that the load applied in the motor and source voltage are constant in time, the motor achieves a steady state. Thus, the electric current and the angular speed become constant

and $\ddot{\alpha}(t) = 0 = \dot{c}(t) = 0$, $\forall t \in \mathbb{R}^{\geq 0}$. By equations (1) and (2), the angular speed of the motor shaft and the current in steady state, respectively $\dot{\alpha}_{steady}$ and c_{steady}, can be calculated by

$$\dot{\alpha}_{steady} = \frac{-\tau\, r + k_t\, v}{b_m\, r + k_e\, k_t} \quad , \quad c_{steady} = \frac{v}{r} - \frac{k_e}{r}\left(\frac{-\tau\, r + k_t\, v}{b_m\, r + k_e\, k_t}\right) . \tag{3}$$

When the hypothesis of constant load is not verified, the angular speed of the motor shaft and the current do not reach a constant value. This kind of situation happens when, for example, a mechanical system is coupled to the motor. In this case, $\dot{\alpha}$ and c variate in time in a way that the dynamics of the motor will be influenced by the coupled mechanical system.

Two more situations are relevant when we analyze electrical motors. The first one is when there is no load applied in the motor (i.e. $\tau(t) = 0$, $\forall t \in \mathbb{R}^{\geq 0}$) and the source voltage is constant in time. Then, the motor achieves its maximum angular speed that is called the *no load speed*. It is calculated by

$$\dot{\alpha}_{no\ load} = \frac{k_t\, v}{b_m\, r + k_e\, k_t} . \tag{4}$$

The second one is when the motor delivers the maximum torque. This torque is achieved when the load applied in the motor is such that the motor does not move at all. This is called the *stall torque*. If the source voltage is constant in time, it is calculated by

$$\tau_{stall} = \frac{k_t\, v}{r} . \tag{5}$$

In the problems discussed here, there is the constraint $\tau(t) < \tau_{stall}$. In Sec. 3 it is taken care do not reach this condition.

2.2 Coupled motor-cart system: a master-slave relation

As described in the introduction, the system analyzed in this paper is composed by a cart whose motion is driven by the DC motor sketched in Fig. 1. The motor is coupled to the cart through a pin that slides into a slot machined on a plexiglas plate that is part to the cart, as shown in Fig. 2. The pin hole is drilled off-center on a disk fixed in the axis of the motor, so that the motor rotational motion is transformed into horizontal cart motion over a rail.

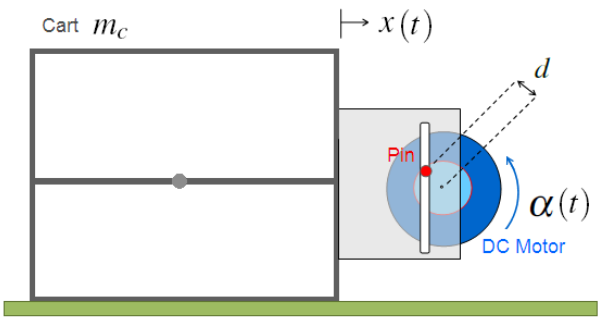

Figure 2: First Mechanical System.

It is noticed that with this configuration, the center of mass of the mechanical system is always located in the center of mass of the cart, so its position does not change.

The mass of the mechanical system, m, is equal the cart mass, m_c, and the horizontal cart displacement is represented by x. Due to constraints, the cart is not allowed to move in the vertical direction. Due to the problem geometry, and noting $||\vec{d}|| = d$, the horizontal motion of the cart and the angular displacement α of the motor are related by the constraint

$$x(t) = d\cos\alpha(t)\ . \tag{6}$$

To model the coupling between the motor and the mechanical system, it is assumed that the motor shaft is rigid. Thus, the available torque to the coupled mechanical system, $\vec{\tau}$, can be written as

$$\vec{\tau}(t) = \vec{d}(t) \times \vec{f}(t)\ , \tag{7}$$

where $\vec{d}$ is the eccentricity of the pin of the motor and $\vec{f}$ is the coupling force between the DC motor and the cart. By the problem geometry, the module of $\vec{d}$ is the nominal eccentricity of the pin. Besides this, the component of $\vec{d}$ that is perpendicular to the plane of the cart movement is always zero and, the others horizontal and vertical components can be calculated from the angular displacement α of the motor.

Assuming that there is no friction between the pin and the slot machined on an acrylic plate, the vector $\vec{f}$ only has a horizontal component, f (the horizontal force that the DC motor exerts in the cart). Thus, $\vec{d}$ and $\vec{f}$ are written as

$$\vec{d}(t) = \begin{bmatrix} d\cos\alpha(t) \\ d\sin\alpha(t) \\ 0 \end{bmatrix} \qquad \vec{f}(t) = \begin{bmatrix} f(t) \\ 0 \\ 0 \end{bmatrix}\ . \tag{8}$$

Substituting Eq. (8) in Eq. (7), the module of $\vec{\tau}(t)$ is

$$\tau(t) = -f(t)d\sin\alpha(t)\ . \tag{9}$$

Since the cart is modeled as a particle, it satisfies the equation

$$m\,\ddot{x} = f(t)\ . \tag{10}$$

Substituting the Eq. (9), (6) and (10) in the equations of the electric motor, we obtain a system of differential equations to the coupled system.

The initial value problem for the motor-cart system is: given the source voltage of the motor, v, find $(\alpha,\ c)$ satisfying

$$\begin{aligned} &l\dot{c}(t) + r\,c(t) + k_e\dot{\alpha}(t) = v\ , \\ &\ddot{\alpha}(t)\ \left[j_m + md^2(\sin\alpha(t))^2\right] + \dot{\alpha}\ \left[b_m + md^2\dot{\alpha}(t)\cos\alpha(t)\ \sin\alpha(t)\right] - k_t\ c(t) = 0\ , \end{aligned} \tag{11}$$

for given initial conditions.

Comparing Eqs. 1, 2, and 11 it is seen that the attached mass influences the motor in a parametric way, [12].

2.3 Coupled motor-cart system with friction

In the model developed to the cart-motor system described in the last subsection, the only mechanism of energy dissipation is associated to the electrical motor. The absence of friction in the mechanical part turns this model unrealistic since the motor can drive the cart for any value of the mass of the mechanical system, m.

Next, it is presented a model to the cart-motor system considering friction between the cart and the rail and in the coupling mechanism, i.e. between the pin and the slot. Therefore, part of the energy provided by the source voltage is dissipated.

As written to the cart-motor system without friction, the available torque to the mechanical system, $\vec{\tau}$, is

$$\vec{\tau}(t) = \vec{d}(t) \times \vec{f}(t) \,, \tag{12}$$

The vector $\vec{f}$ has a horizontal component, f_x, that is the horizontal force that the DC motor exerts in the cart, and has a vertical component, f_y, that is the vertical force that the DC motor exerts in the cart due to friction between the pin and the slot. Thus, $\vec{d}$ and $\vec{f}$ are written as

$$\vec{d}(t) = \begin{bmatrix} d\cos\alpha(t) \\ d\sin\alpha(t) \\ 0 \end{bmatrix} \qquad \vec{f}(t) = \begin{bmatrix} f_x(t) \\ f_y(t) \\ 0 \end{bmatrix} . \tag{13}$$

Substituting Eq. (13) in Eq. (12), the module of $\vec{\tau}(t)$ is

$$\tau(t) = f_y(t)\, d\cos\alpha(t) - f_x(t)\, d\sin\alpha(t) \,. \tag{14}$$

The friction in the couple mechanism makes a vertical friction force, fat_c, in the pin. The adopted model to this force is

$$fat_c(t) = -\,|f_x(t)|\,\mu_1\ \mathrm{sgn}\left(\dot{\alpha}\cos\left(\alpha(t)\right)\right) , \tag{15}$$

where μ_1 is the coefficient friction between the pin and the slot and the term $\mathrm{sgn}\left(\dot{\alpha}\cos\left(\alpha(t)\right)\right)$ indicates the sign of the pin velocity. The vertical force that the DC motor exerts in the cart is

$$f_y(t) = -fat_c(t) \,. \tag{16}$$

The friction force between the cart and the rail is written as

$$fat_r(t) = -\,|n(t)|\,\mu_2\ \mathrm{sgn}\left(\dot{x}(t)\right) , \tag{17}$$

where n is the normal force exerted by the rail in the cart, μ_2 is the coefficient between the cart and the rail. Since the cart is modeled as a particle, its movement in the horizontal direction satisfies the equation

$$m\,\ddot{x} = f_x(t) + fat_r(t) \,, \tag{18}$$

and since the cart is not allowed to move in the vertical direction, the sum of all forces acting on the cart in the vertical direction must be zero, i.e.

$$0 = n(t) - m\,g + f_y(t) \,, \tag{19}$$

where g is the gravitational acceleration.

Substituting the Eq. (14), (15), (16) and (17) in the equations of the electric motor, and considering Eq. (18), (19), we obtain a system of differential algebraic equations to the coupled motor-cart system with friction.

The initial value problem is: given v, find $(\alpha,\ c)$ satisfying

$$
\begin{aligned}
& l\dot{c} + r\,c + k_e\dot{\alpha} = v\ , \\
& j_m\ddot{\alpha} + b_m\dot{\alpha} - k_t c = -\,|f_x|\,\mu_1\ \operatorname{sgn}(\dot{\alpha}\cos\alpha)d\cos\alpha + f_x d\sin\alpha\ , \\
& m(-\ddot{\alpha}d\sin\alpha - (\dot{\alpha})^2 d\cos\alpha) = f_x + |n|\,\mu_2\ \operatorname{sgn}(\dot{\alpha}\sin\alpha)\ , \\
& 0 = n - mg + |f_x|\,\mu_1\ \operatorname{sgn}(\dot{\alpha}\cos\alpha)\ ,
\end{aligned}
\tag{20}
$$

for given initial conditions.

2.4 Coupled motor-cart-pendulum system: introduction of a mechanical energy reservoir

In the second system, a third element, a pendulum, is attached to the cart. It is placed inside the cart, as shown in Fig. 3. The suspension point O is fixed in the cart, hence moves with it. The important point is that it can have a relative motion with respect to the cart. That is the meaning we give to *embarked*.

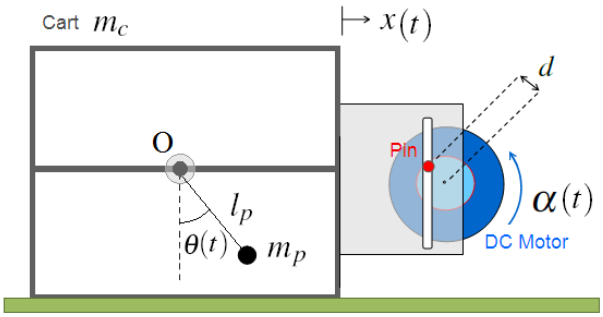

Figure 3: Second Mechanical System.

The embarked pendulum is modeled as a mathematical pendulum (bar without mass and particle of mass m_p at the end). The pendulum length is represented by l_p and the pendulum angular displacement by θ.

Using the Lagrangian equation $\mathcal{L} = \mathcal{T} - \mathcal{V}$, with the angle θ and displacement x of the cart as generalized coordinates, the kinetic and potential energies of the mechanical system, are defined respectively as

$$
\mathcal{T} = \frac{1}{2}m_p[(l_p\dot{\theta}\cos\theta + \dot{x})^2 + (l_p\dot{\theta}\sin\theta)^2] + \frac{1}{2}m_c\dot{x}^2\ , \tag{21}
$$

$$
\mathcal{V} = -m_p g(l_p\cos\theta)\ . \tag{22}
$$

Thus, the equation of the cart-pendulum are

$$
m_p l_p^2\ddot{\theta}(t) + m_p l_p\ddot{x}(t)\cos\theta(t) + m_p g l_p\sin\theta(t) = 0\ , \tag{23}
$$

$$(m_p + m_c)\ddot{x}(t) + m_p l_p \ddot{\theta}(t)\cos\theta(t) - m_p l_p \dot{\theta}^2(t)\sin\theta(t) = f(t)\ , \tag{24}$$

where, again, f represents the horizontal coupling force between the DC motor and the cart, g is the gravity and the horizontal cart displacement is x.

The relative motion of the embarked pendulum causes a variation in the position of the center of mass of the mechanical system. In this case, the mass of the mechanical system, m, is equal the cart mass plus the pendulum mass, $m_c + m_p$.

As in the first coupled system, the cart is not allowed to move in the vertical direction. Due to the problem geometry, the horizontal motion of the cart and the angular displacement α of the motor are related by Eq. (6).

Once again, it is assumed that the motor shaft is rigid and that there is no friction between the pin and the slot machined on the acrylic plate. Thus, the available torque to the coupled mechanical system, $\vec{\tau}$, is written as Eq. (9).

Substituting the Eq. (9), (6) and (24) in the equations of the electric motor and in Eq. (23), we obtain a system of differential equations for the coupled system.

Given the source voltage of the motor, v, the dynamic of the coupled system is written in terms of the variables α, c and θ. Thus, the initial value problem for the motor-cart-pendulum system is: given the source voltage of the motor, v, find $(\alpha,\ c,\ \theta)$ satisfying

$$\begin{aligned}
&l\dot{c}(t) + rc(t) + k_e\dot{\alpha}(t) = v\ ,\\
&\ddot{\alpha}(t)\ \left[j_m + (m_c+m_p)d^2(\sin\alpha(t))^2\right] +\ \dot{\alpha}(t)\ \left[b_m + (m_c+m_p)d^2\dot{\alpha}(t)\cos\alpha(t)\ \sin\alpha(t)\right] +\\
&\qquad +k_t\ c(t)\ -\ \ddot{\theta}(t)\ [m_p l_p\cos\theta(t) d\sin\alpha(t)] + \dot{\theta}(t)\ \left[m_p\ l_p\dot{\theta}(t)\sin\theta(t) d\sin\alpha(t)\right] = 0\ ,\\
&\ddot{\theta}(t)\ \left[m_p\ l_p^2\right] - \ddot{\alpha}(t)\ [m_p\ l_p\ \cos\theta(t) d\sin\alpha(t)] -\ \dot{\alpha}(t)\ [m_p\ l_p\cos\theta(t) d\cos\alpha(t)\dot{\alpha}(t)] +\\
&\qquad\qquad + m_p\ g\ l_p\sin\theta(t)\ =\ 0\ ,
\end{aligned} \tag{25}$$

for given initial conditions.

2.5 Coupled motor-cart-pendulum system with friction

Next, it is presented a model to the motor-cart-pendulum system considering friction between the cart and the rail and in the coupling mechanism, i.e. between the pin and the slot.

As written to the motor-cart-pendulum system without friction, the module of the available torque to the mechanical system, $\vec{\tau}$, is

$$\tau(t) = f_y(t)\ d\cos\alpha(t) - f_x(t)\ d\sin\alpha(t)\ . \tag{26}$$

where f_x is the horizontal component of the force that the DC motor exerts in the cart and f_y is its vertical component. The friction in the couple mechanism makes a vertical friction force, fat_c, in the pin. The adopted model to this force is equal to the model adopted in the motor-cart system with friction, i.e.

$$fat_c(t) = -\left|f_x(t)\right|\mu_1\ \mathrm{sgn}\left(\dot{\alpha}\cos\left(\alpha(t)\right)\right)\ , \tag{27}$$

where again μ_1 is the coefficient friction between the pin and the slot and the term $\text{sgn}(\dot{\alpha}\cos(\alpha(t)))$ indicates the sign of the pin velocity. The vertical force that the DC motor exerts in the cart is

$$f_y(t) = -fat_c(t) \, . \tag{28}$$

The friction force between the cart and the rail is written as

$$fat_r(t) = -|n(t)|\,\mu_2\ \text{sgn}(\dot{x}(t)) \, , \tag{29}$$

where again n is the normal force exerted by the rail in the cart, μ_2 is the friction coefficient between the cart and the rail.

Using the Lagrangian equation, the obtained equation of the cart-pendulum is

$$m_p l_p^2 \ddot{\theta}(t) + m_p l_p \ddot{x}(t)\cos\theta(t) + m_p g l_p \sin\theta(t) = 0 \, , \tag{30}$$

$$(m_p + m_c)\ddot{x}(t) + m_p l_p \ddot{\theta}(t)\cos\theta(t) - m_p l_p \dot{\theta}^2(t)\sin\theta(t) = f_x(t) + fat_r(t) \, , \tag{31}$$

Since the cart is not allowed to move in the vertical direction, the sum of all forces acting on the cart in the vertical direction must be zero. Thus the sum of the normal force exerted by the rail in the cart, the gravitational force, the vertical force f_y and the vertical component of the force exerted by the pendulum in the cart must be zero, i.e.

$$0 = n(t) - (m_c + m_p)\, g + f_y(t) + m_p l_p \ddot{\theta}(t)\sin(\theta(t)) + m_p l_p \dot{\theta}^2(t)\cos(\theta(t)) \, . \tag{32}$$

Substituting the Eq. (26), (27), (28) and (29) in the equations of the electric motor, and considering Eq. (30), (31) and (32), we obtain a system of differential algebraic equations to the coupled motor-cart-pendulum system with friction.

The initial value problem is: given v, find $(\alpha,\, c)$ satisfying

$$\begin{aligned}
&l\dot{c} + r\,c + k_e\dot{\alpha} = v \, , \\
&j_m\ddot{\alpha} + b_m\dot{\alpha} - k_t c = -|f_x|\,\mu_1\ \text{sgn}(\dot{\alpha}\cos\alpha) d\cos\alpha + f_x d\sin\alpha \, , \\
&\ddot{\theta}\ \left[m_p\, l_p^2\right] - \ddot{\alpha}\ \left[m_p\, l_p\ \cos\theta d\sin\alpha\right] - \ \dot{\alpha}\ \left[m_p\, l_p \cos\theta d\cos\alpha\dot{\alpha}\right] + \ m_p\, g\, l_p \sin\theta\ = \ 0 \, , \\
&m(-\ddot{\alpha}d\sin\alpha - (\dot{\alpha})^2 d\cos\alpha) + m_p l_p \ddot{\theta}\cos(\theta) + m_p l_p \dot{\theta}^2 \sin(\theta) = f_x + |n|\,\mu_2\ \text{sgn}(\dot{\alpha}\sin\alpha) \, , \\
&0 = n - (m_c + m_p)g + |f_x|\,\mu_1\ \text{sgn}(\dot{\alpha}\cos\alpha) + + m_p l_p \ddot{\theta}\sin(\theta) + m_p l_p \dot{\theta}^2\cos(\theta) \, ,
\end{aligned} \tag{33}$$

for given initial conditions.

3 NUMERICAL SIMULATIONS OF THE DYNAMICS OF THE COUPLED SYSTEMS

To better comprehend the behavior of the coupled system composed by the DC motor and the mechanical systems, we started analyzing the deterministic models. Simulations of the two systems are compared in order to observe the influence of the pendulum in the rotational motion of the motor shaft.

3.1 Simulations of the motor-cart system

Looking at the initial value problem Eq. (11), it is observed that if the nominal eccentricity of the pin, d, is small, Eq. (11) tends to the linear system equations of the DC motor, Eq. (1) and (2), in case of no load. But as the eccentricity grows, the non-linearities become more pronounced. The nonlinearity also increases with the attached mass, m. To better comprehend the increase of nonlinearity, the system Eq. (11), was integrated in a range of $[0.0,\ 2.0]$ seconds for different values of d and m.

The specifications of the motor parameters used in all simulations were obtained from the specifications of the motor Maxon DC brushless number 411678. The source voltage was assumed to be constant in time and equal to 2.4 [Volt]. This value is just 10% of the nominal voltage of this motor, 24 [Volt], but it ensures the respect to the constraint $\tau(t) < \tau_{stall}$ for the parameters considered for the coupled system. So the simulations reflect realizable situations.

In the integration, the initial conditions assumed for the current in the motor and for the angular position and velocity of the motor shaft were, in all simulations:

$$\alpha(0) = 0.0 \text{ [rad]}\,, \qquad \dot{\alpha}(0) = 0.0 \text{ [Hz]}\,, \qquad c(0) = v/r = 7.81 \text{ [Amp]}\,. \tag{34}$$

Due to the coupling mechanism, coupling torque, τ, variates in time. Thus, the angular speed of the motor shaft and the current are not constant values after the transient. As the motor-cart system does not have any mechanism of storing energy, after the transient the dynamics achieves a periodic state.

To study the variation of the motor current, the coupling force and torque, the mass was fixed to 5 [Kg] and two values of d were selected: 0.001 [m] and 0.010 [m]. The selection guarantees that the stall torque is not reached in the simulations.

The Fast Fourier Transform of the cart displacement over time, $\hat{x}$, was computed for the two different values of d. Figures 4(b) and 5(b) show the obtained results. It is noted that when d is small, as 0.001 [m], the angular speed of the motor shaft oscillates with a small amplitude around 7 [Hz] and the FFT graph of x presents only one peak at this frequency. In contrast to this, when d is bigger, the amplitude of the oscillations of $\dot{\alpha}$ grows and, due to the non-linearity effects, the FFT graph of x presents more than one peak. The first one of them is at 6.56 [Hz] and, the following are at odd multiples of this value.

As said in the introduction of this paper, normally problems of coupled systems are modeled saying that the force is imposed, so no coupling, and it is harmonic with frequency given by the nominal frequency of the motor. The dynamic of the motor is not considered. The graphs of Fig. 4(a) and 5(a) confirm that this hypothesis does not correspond to reality. Even when d is small, the angular speed of the motor shaft do not reach a constant value. After a transient it achieves a periodic state. It oscillates around a mean value and these oscillations are periodic.

Others graphs to be analyzed are the $f(t)$ and $\tau(t)$ variation during one n-th cart movement cycle. This type of graph will be called *phase portrait*. The Fig. 6(a) and 6(b) shows these graphs for the fourth cycle, i.e., $n = 4$ and $\alpha(t) \in [8\pi, 10\pi]$.

Observing the f graph and remembering the constrain $x(t) = d\cos\alpha(t)$, it is verified that the horizontal force presents its maximum value when $x(t) = -d$ [m] and its minimum value when $x(t) = d$ [m]. Besides this, the cart positions corresponding to the points where f changes sign are $x(t) = -0.00415$ [m] and $x(t) = 0.00415$ [m]. At this values, the angular positions of the motor shaft, in the n-th cart movement cycle, are equals to $\alpha(t) = n2\pi + 1.99$ [rad] and $\alpha(t) = n2\pi + 5,14$ [rad].

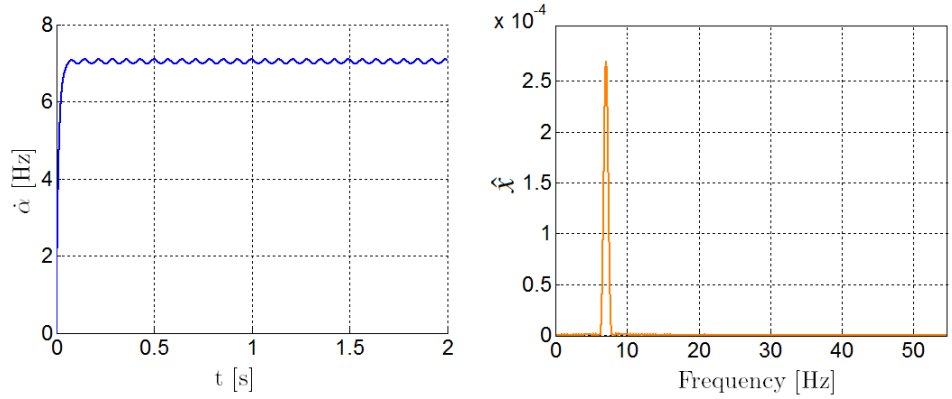

(a) (b)

Figure 4: Motor-cart system $d = 0.001$ [m]: (a) angular speed of the motor shaft over time and (b) Fast Fourier Transform of the cart displacement.

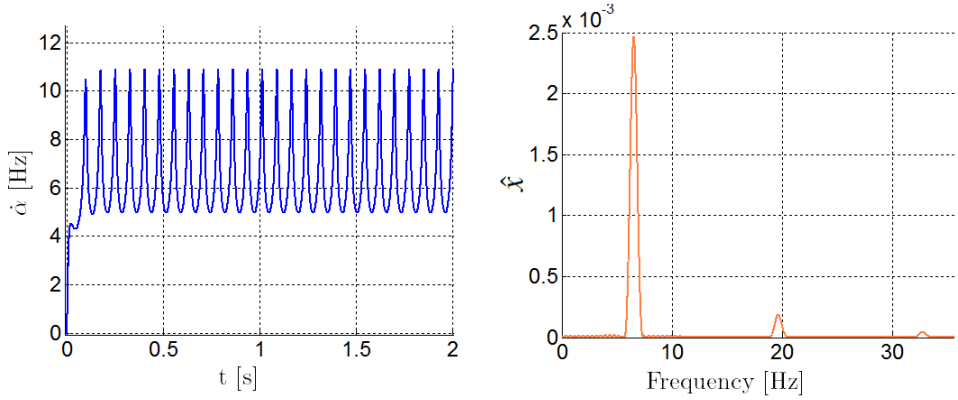

(a) (b)

Figure 5: Motor-cart system $d = 0.01$ [m]: (a) angular speed of the motor shaft over time and (b) Fast Fourier Transform of the cart displacement.

Observing the τ graph, it is verified that the torque presents four points of sign changes. Two of them occur when $x(t) = -d$ and $x(t) = d$, corresponding respectively to α multiple of π and α multiple of 2π. This changes were expected from Eq. (9). The others two changes occur exactly in the same cart positions that we have the f sign changing, i.e., when $x(t) = -0.00415$ [m] and $x(t) = 0.00415$ [m]. In each cart movement cycle, the horizontal force f and the torque τ follow once the paths shown in Fig. 6(a) and 6(b).

The Fig. 7(a) and 7(b) show the graphs of the current variation during the fourth cart movement cycle and the torque variation in function of the current. In the left graph, it is noted that the current presents four points of sign changing. They occur when the x value are 0.00891 [m], -0.00728 [m], -0.00891 [m] and 0.00728 [m]. The corresponding angular positions of the motor shaft in the n-th cart movement cycle, α, at these points are $n2\pi + 0.47$ [rad], $n2\pi + 2.38$ [rad], $n2\pi + 3.61$ [rad] and $n2\pi + 5.53$ [rad].

3.2 Simulations of the motor-cart system with friction

Looking at the system of differential algebraic equations to the coupled motor-cart system with friction, Eq. (20), it is possible observe that the two frictions forces considered in the

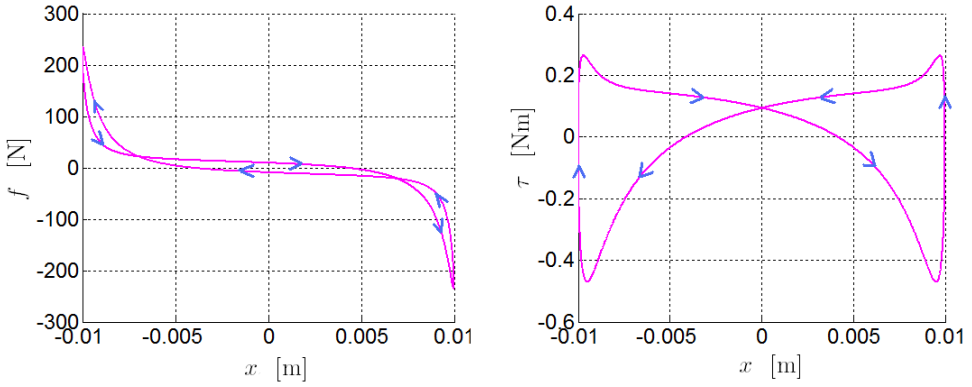

(a) (b)

Figure 6: Motor-cart system with $d = 0.01$ [m]: (a) horizontal force f and (b) torque τ during one cycle of the cart movement.

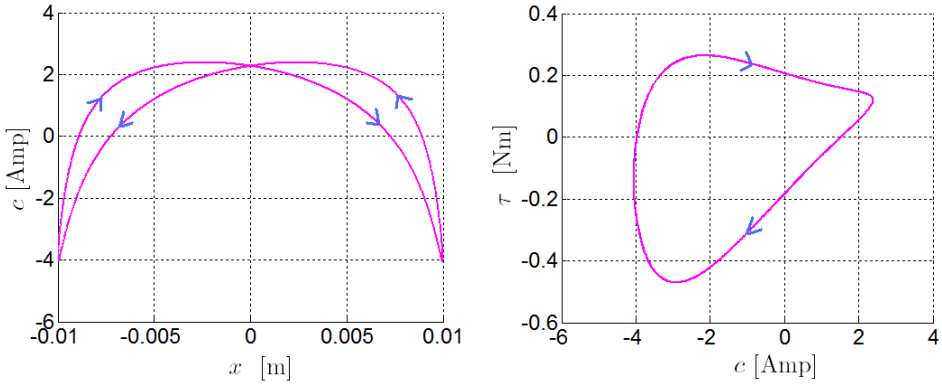

(a) (b)

Figure 7: Motor-cart system with $d = 0.01$ [m]: (a) current variation during the fourth cart movement cycle and (b) torque variation in function of the current.

problem are coupled, i.e. there is mutual influence between them.

To better understand the influence of each friction force in the system and the effects of the coupling between them, Eq. (20) was integrated numerically in a range of $[0.0,\ 3.0]$ seconds in tree different situations. In the first one, it was considered the existence of friction only in the coupling mechanism. In the second one, it was considered the existence of friction only between the cart and the rail and, in the third one, the two frictions were considered.

In all simulations, the values used to the initial conditions for the angular position and velocity of the motor shaft were $\alpha(0) = \dot{\alpha}(0) = 0.0$, and for the current in the motor was $c(0) = v/r = 7.81$ [Amp]. The specifications of the motor parameters were equal to the ones used in the previous integrations. The source voltage was assumed to be constant in time and equal to 2.4 [Volt]. The values of the mass and nominal eccentricity of the pin were $m = 5.0$ [Kg] and $d = 0.010$ [m].

The values of the friction coefficients were obtained from [13]. It was assumed that the pin is made of steel and the slot is machined on a plexiglas plate. The used value to the friction coefficient in the coupling mechanism was $\mu_1 = 0.4$. To determine the second friction coefficient, it was assumed that the cart is made of steel and the rail made of cast iron. The used value to μ_2 was 0.1.

Next are shown the results of the integration of Eq. (20) considering the existence of friction only in the coupling mechanism. As in the previous simulations, due to the coupling mechanism, the coupling torque, τ, variates in time. Thus, the angular speed of the motor shaft and the current are not constant values after the transient. Despites the consideration of friction, after a transient period the dynamics achieves a periodic state that can be observed in Fig. 8(a) and 8(b).

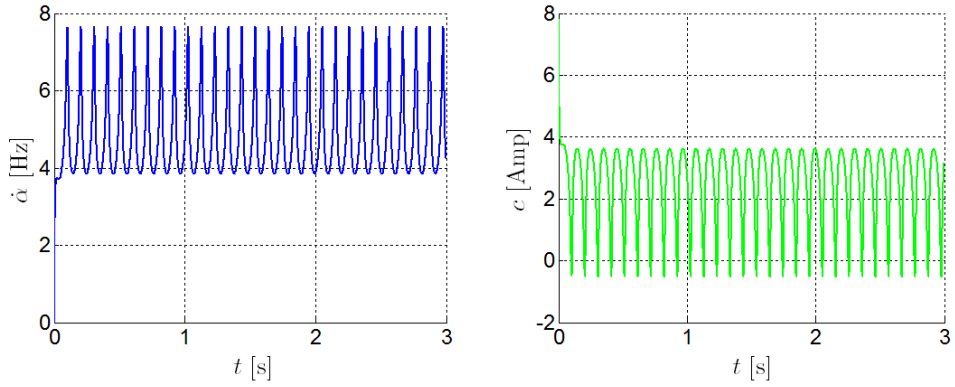

(a) (b)

Figure 8: Motor-cart system with friction in the coupling mechanism: (a) angular velocity of the motor shaft and (b) current over time.

The phase portraits of the horizontal and vertical forces during one cycle of the cart movement are shown in Fig. 9(a) and 9(b). Comparing the graph of f_x with Fig. 6(a) it is possible observe that the horizontal force does not presents anymore its maximum and minimum value at the extremities positions of the cart trajectory. They occur at $x(t) = -0.00957$ [m] and $x(t) = 0.00957$ [m]. Besides this, the cart positions corresponding to the points where f_x changes sign were also modified. They occur at $x(t) = -0.00518$ [m] and $x(t) = 0.00518$ [m].

The graph of f_y presents its minimum value at $x(t) = -0.00957$ [m], its maximum value at $x(t) = 0.00957$ and presents a discontinuity at $x(t) = 0.0$ [m]. This discontinuity occurs because at this position, the friction force in the coupling mechanism changes its sign due to the term $\text{sgn}(\dot{\alpha}\cos(\alpha(t)))$ that appears in Eq. (15) and because $f_y(t) = -fat_c(t)$, see Eq. (16). Another characteristic of this graph is that f_y is zero at the same positions that occurs the sign changing of f_x ($x(t) = 0.00518$ [m] and $x(t) = 0.00518$ [m]). This result is expected since the friction force in the coupling mechanism is proportional to the module of f_x, see Eq. (15).

Figures 10(a) and 10(b) show the normal force and coupling torque during one cycle of the cart movement.

The results of the integration of Eq. (20) considering the existence of friction only between the cart and the rail are presented next. Figures 11(a) and 11(b) show the phase portrait graphs to the horizontal force and torque. Comparing the graph of f_x with Fig. 8(a) it is possible observe that different to the previous case, the horizontal force presents its maximum and minimum value at the extremities positions of the cart trajectory. The cart positions corresponding to the points where f_x changes sign are at $x(t) = -0.00526$ [m] and $x(t) = 0.00526$ [m].

Next are presented the results of the integration of Eq. (20) considering the two friction forces, in the coupling mechanism and between the cart and the rail. Figures 12(a) and 12(b) show the phase portraits of the horizontal and vertical forces. Comparing these graphs with the previous phase portraits of the coupling forces, Fig. 9(a) and 9(b), it is possible observe that

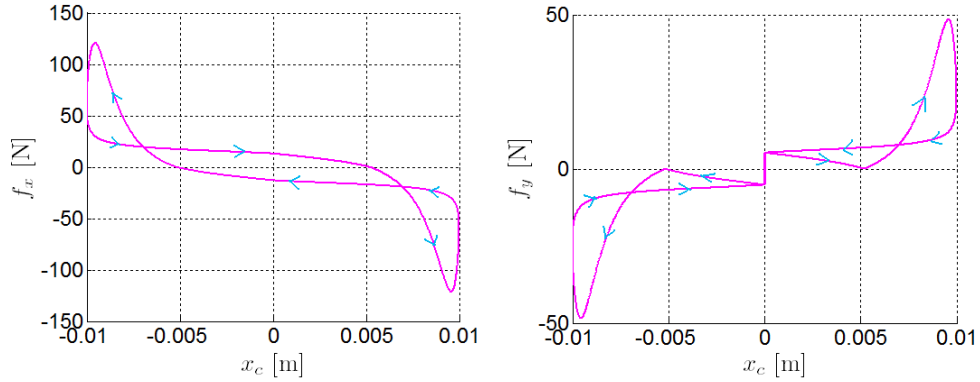

(a) (b)

Figure 9: Motor-cart system with friction in the coupling mechanism: (a) horizontal and (b) vertical forces during one cycle of the cart movement.

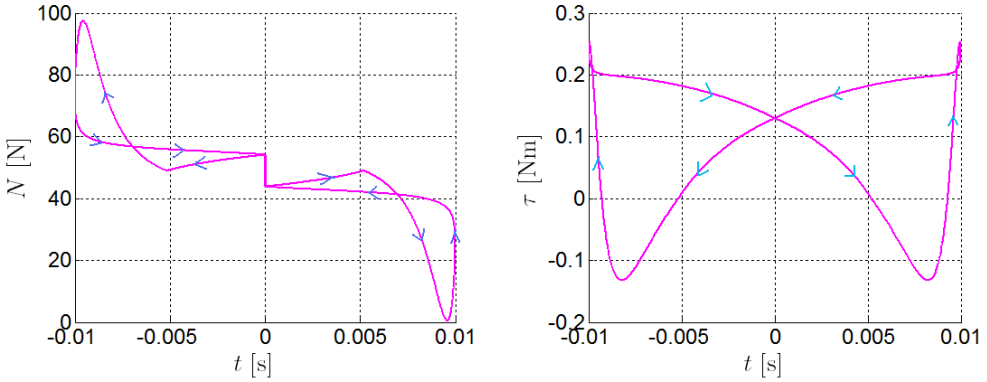

(a) (b)

Figure 10: Motor-cart system with friction in the coupling mechanism: (a) normal force and (b) torque during one cycle of the cart movement.

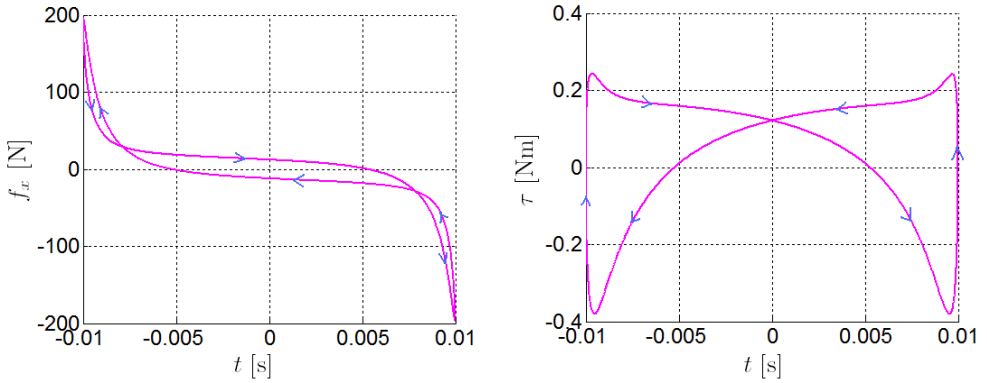

(a) (b)

Figure 11: Motor-cart system with friction between the cart and rail: (a) horizontal force and (b) torque during one cycle of the cart movement.

they present similar shapes to the previous ones but they have lost their symmetry in relation to the maximum and minimum values of the forces. For example, the maximum horizontal force

in the new phase portrait is 96.7 [N] and the minimum is −105.9 [N].

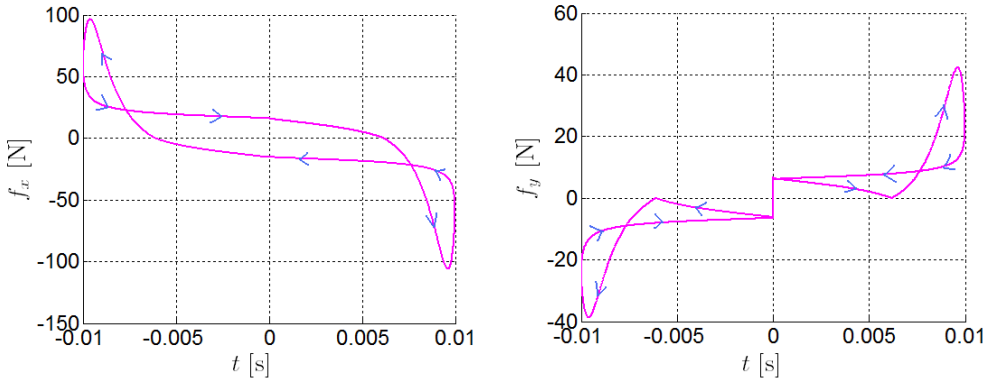

(a) (b)

Figure 12: Motor-cart system with friction in the coupling mechanism and between the cart and rail: (a) horizontal and (b) vertical forces during one cycle of the cart movement.

The same phenomenon occurs with the phase portraits of the friction forces, fat_c and fat_r, shown in Fig. 13(a) and 13(b).

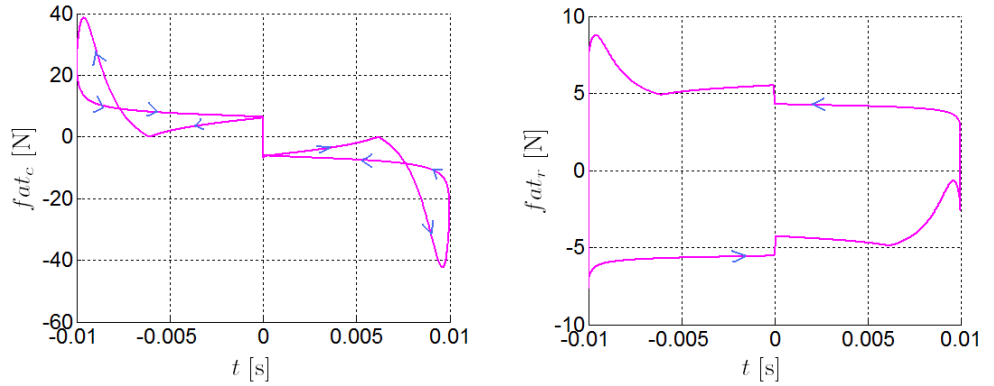

(a) (b)

Figure 13: Motor-cart system with friction in the coupling mechanism and between the cart and rail: friction (a) in the coupling mechanism and (b) between the cart and the rail during one cycle of the cart movement.

Figures 14(a) and 14(b) show the phase portraits of the normal force and the coupling force. In the graph of τ is possible observe that there is a discontinuity at $x(t) = 0.0$ [m] due to discontinuity that exists in phase graph of f_y at this position.

The lost of symmetry in the phase portraits in the case that the two frictions are considered is due to difference of the nature of the forces acting on the cart in horizontal and vertical direction, see Eq. (18) and (19). While in the balance of horizontal forces there are only dynamic forces (f_x and fat_r), in the balance of vertical forces there are two types of forces, dynamics (f_y and n) and constant (the weight $m\,g$).

To verify this, one simple test was donne. In the the integration of Eq. (20), the value of acceleration of gravity was assumed to be equal to zero, making vanish the weight force in Eq. (19). As result, all the phase diagrams became symmetrical.

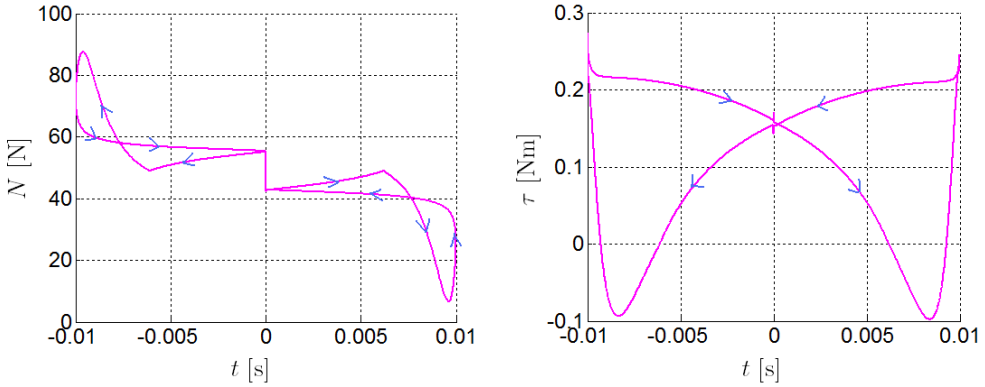

(a) (b)

Figure 14: Motor-cart system with friction in the coupling mechanism and between the cart and rail: (a) normal force and (b) torque during one cycle of the cart movement.

3.3 Simulations of the motor-cart-pendulum system

A similar analysis to the one made to the motor-cart system was developed for the motor-cart-pendulum system.

Looking at the initial value problem Eq. (25), it is observed that if the nominal eccentricity of the pin, d, is small and the angle $\theta(t)$ is near zero, Eq. (25) tends to a linear system. But as the eccentricity grows, the nonlinearities become more pronounced. To better comprehend the increase of nonlinearities, the system Eq. (25), was integrated in a range of [0.0, 50.0] seconds for two different values of d: 0.001 [m] and 0.010 [m].

It was considered as initial conditions for the angular position and velocity of the motor shaft, $\alpha(0) = \dot{\alpha}(0) = 0.0$, and for the current in the motor $c(0) = v/r = 7.81$ [Amp] and for the angular position and velocity of the pendulum $\theta(0) = \dot{\theta}(0) = 0.0$. The specifications of the motor parameters used in the simulations are equal to the ones used in the simulations of the motor-cart system. The source voltage was assumed to be constant in time and equal to 2.4 [Volt]. The values of the cart and the pendulum masses were $m_c = 0.0$ [Kg] and $m_p = 5.0$ [Kg], so that the total mass, $m = m_c + m_p = 5.0$ [Kg], is equal to the embarked mass. Although the masses are equal, this configuration contrasts with the one of the motor-cart system used in the previous simulations. In spite of having the same masses, the pendulum has a relative motion with respect to the cart, and this make a huge difference. The pendulum length was assumed to be 0.075 [m].

The results obtained with the integration of Eq. (25), considering $d = 0.001$ [m], are shown in Fig. 15(a) and 15(b). These results reveal that when d is small, the angular speed of the motor shaft oscillates over time with a very small amplitude around 7 [Hz] and the current also oscillates with a small amplitude around 0.13 [Amp].

When d is bigger, the amplitude of the oscillations of $\dot{\alpha}$ is bigger when compared with the result obtained with the smaller d. Figures 16(a) and 16(b) show the angular speed of the motor and angular displacement pendulum over time as result to the integration of Eq. 25 with $d = 0.01$ [m].

The presence of the pendulum, that is a mechanism energy reservoir, presents reflects in the graphs of f and τ during one cart movement cycle. Figures 17(a) and 17(b) show these two graphs for the last cycle in the period $[0,\ 50]$ seconds of the integration of Eq. 25. It is possible to observe that the graphs of τ and f have lost their symmetry in relation to a vertical axis drawn

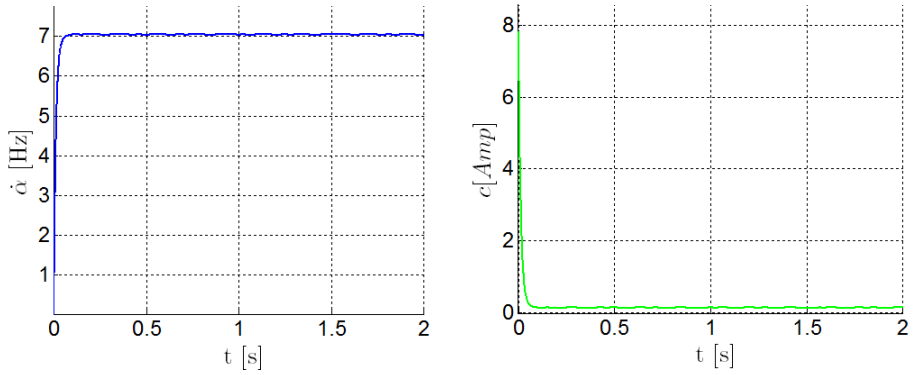

(a) (b)

Figure 15: Motor-cart-pendulum system with $d = 0.001$ [m]: (a) angular velocity of the motor shaft and (b) current over time.

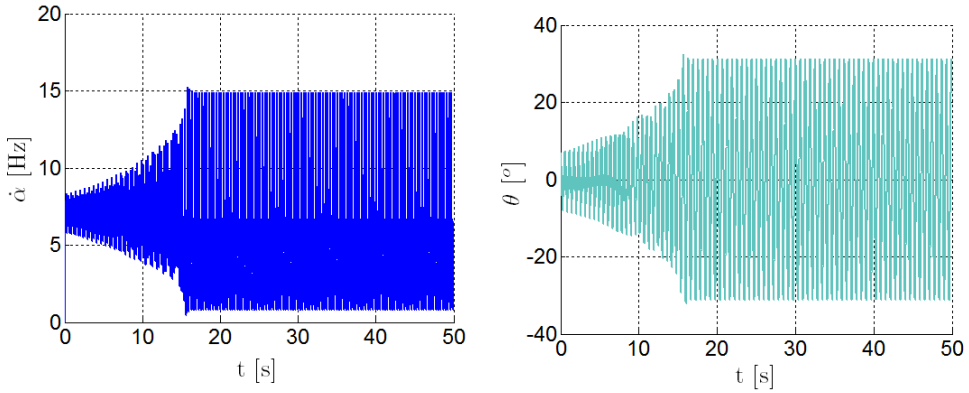

(a) (b)

Figure 16: Motor-cart-pendulum system with $d = 0.01$ [m]: (a) angular velocity of the motor shaft and (b) pendulum displacement over time.

at $x = 0$. Thus, the pendulum changes the dynamic behavior of the cart and of the motor. More details could be found in [14] and [15].

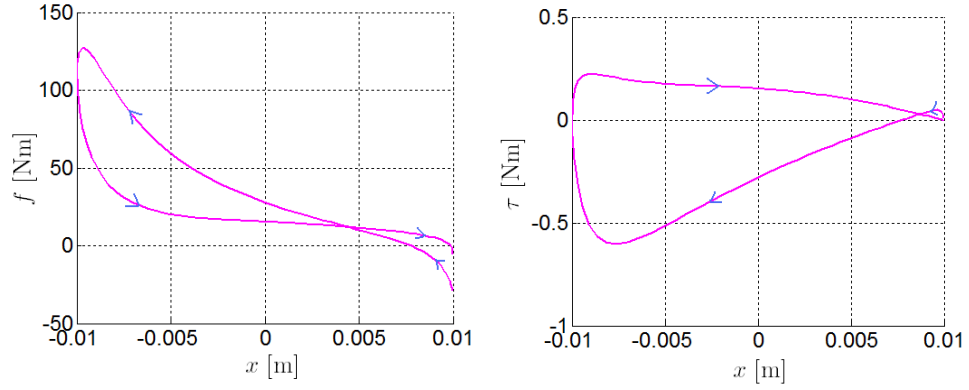

(a) (b)

Figure 17: Motor-cart-pendulum system with $d = 0.01$ [m]: (a) horizontal force f and (b) torque τ during the last cycle of the cart movement.

3.4 Simulations of the motor-cart-pendulum system: pumping leads to revolution

In the analysis developed to the the motor-cart-pendulum system, in the previous section of the paper, the cart mass was considered to be zero and the pendulum mass 5.0[Kg]. Next, it is presented an analysis of the behavior of this system with a different mass configuration. The cart mass is kept as 0.0 [Kg] and a smaller value is selected to the pendulum mass, $m_p = 4.0$ [Kg], so that the total mass, $m_c + m_p = 4.0$ [Kg], is still equal to the embarked mass.

To observe the influence of this new configuration in the system behavior, the Eq. 25 was integrated in a range of $[0,\ 50]$ seconds with the null initial conditions to $\alpha(0)$, $\dot{\alpha}(0)$, $\theta(0)$ and $\dot{\theta}(0)$. The initial current was considered equal to $c(0) = v/r = 7.81$ [Amp] and the nominal pin eccentricity 0.01 [m]. The source voltage was assumed to be constant in time and the specifications of the motor parameters were equal to the used in the previous simulations

The obtained results for the angular speed of the motor shaft, for the current and cart and pendulum displacements are shown in Fig. 18(a), Fig. 18(b), Fig. 19(a) and Fig. 19(b). The mechanical system pumps energy from the motor and the amplitude of the pendulum grows reaching a point where the mechanical system starts to drive the motion, [16, 17, 18]. This is seen nothing that $\dot{\alpha}$ takes negatives values, meaning that the motor shaft changes its motion direction sometimes. When the angular speed of the motor shaft is positive, it is considered that the motor drives the cart motion, the cart is driven. But in the period when it is negative, the motor looses the control over the cart and drives it no more, it is now driven by the mechanical system. In these situations, it will be said that the relation master-slave is reverted.

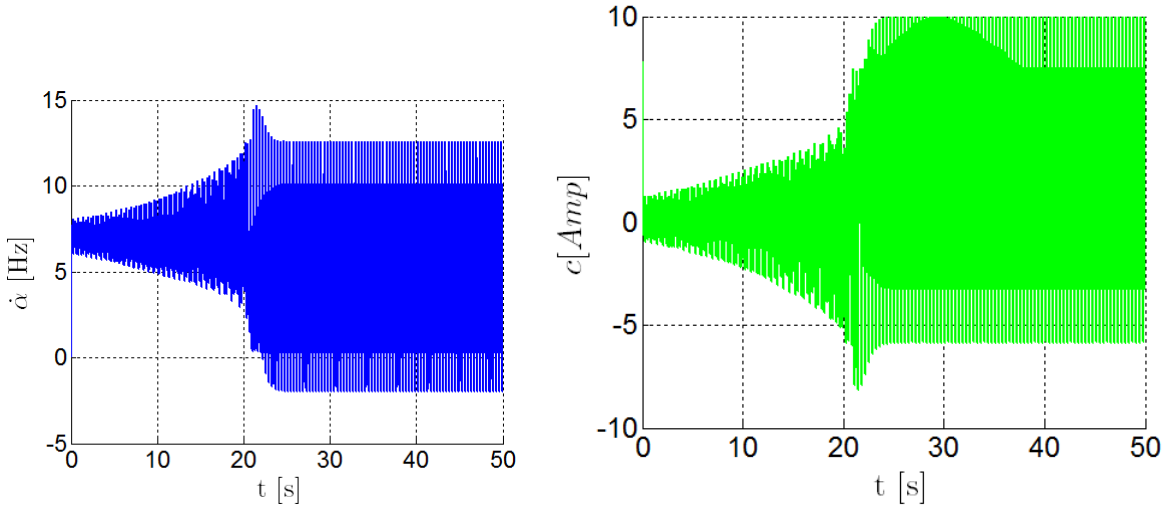

(a) (b)

Figure 18: Motor-cart-pendulum system with $d = 0.01$ [m]: (a) angular velocity of the motor shaft and (b) current over time.

To better comprehend the sign changing of the angular speed of the motor shaft, some phase portrait graphs were plotted. Figures 20(a) and 20(b) show the $\ddot{\alpha}$ graph in function of $\dot{\alpha}$ and the $\dot{\alpha}$ graph in function of x during one movement cycle. It is verified that when $\dot{\alpha}(t)$ turns negative, the motor shaft has a negative acceleration. After a short period of time, its acceleration becomes positive and brakes the motor shaft motion. This causes other sign changing in $\dot{\alpha}(t)$ and consequently, it turns positive again. Thus, the motor recovers the control over the cart motion.

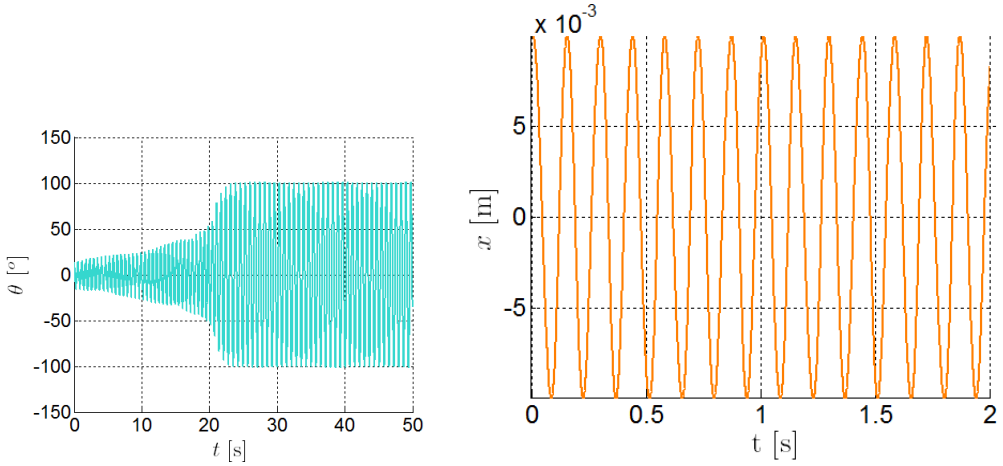

(a) (b)

Figure 19: Motor-cart-pendulum system with $d = 0.01$ [m]: (a) pendulum and (b) cart displacement over time.

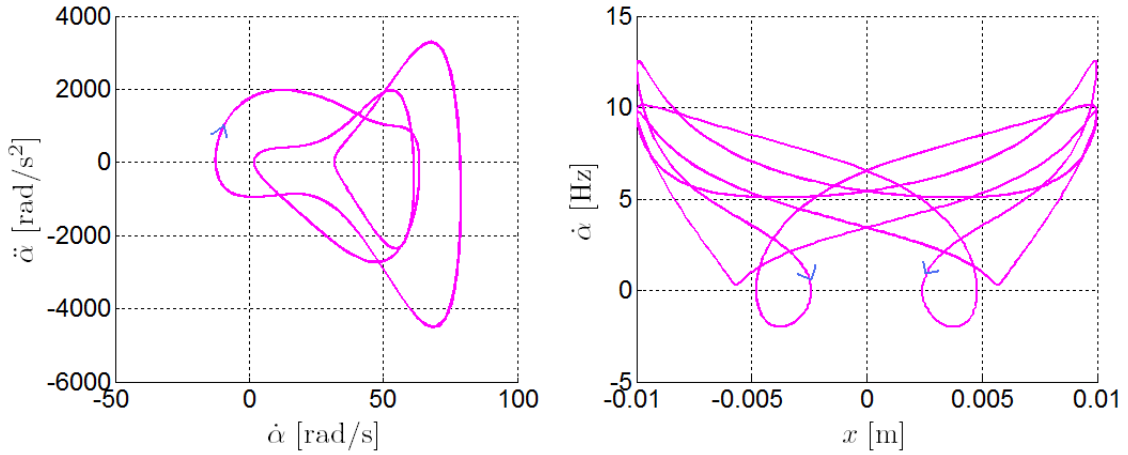

(a) (b)

Figure 20: Motor-cart-pendulum system with $d = 0.01$ [m]: portrait graphs of (a) $\ddot{\alpha}$ graph in function of $\dot{\alpha}$ and (b) $\dot{\alpha}$ graph in function of x.

Looking at Fig. 20(b), it is noted that this reversion in the relation master-slave occurs two times in each movement cycle. The position and angular speed of the pendulum, at the moment of the reversion, can be discovered by the graphs of $\dot{\theta}$ in function of $\dot{\alpha}$ and θ in function of $\dot{\alpha}$. They are shown in Fig. 21(a) and 21(b). It is verified that when the the motor looses the control over the cart by the sign changing of $\dot{\alpha}$, the pendulum angle is around 21.6 [^{o}] or around -21.6 [^{o}]. When the motor recovers the control, the pendulum angle is around 6.0 [^{o}] or around -6.0 [^{o}].

It is also noted that, during the period of reversion, the pendulum does not change its direction of motion in spite of its angular speed presents a change of behavior. In the beginning of the reversion the modulus of $\dot{\theta}$ grows, but when it achieves the value 2.95 [Hz], it starts to decrease. This change occurs due to the sign changing in the tangent angular acceleration of the pendulum, as can be observed in Fig. 22(a). The graph of the torque variation in function of the angular speed of the motor shaft shows that the maximum torque is achieved during the period of reversion.

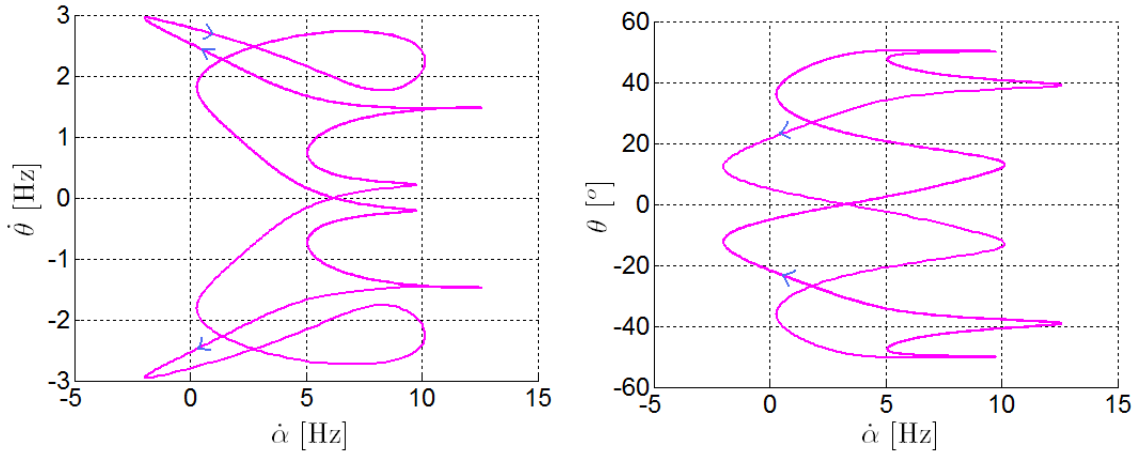

(a) (b)

Figure 21: Motor-cart-pendulum system with $d = 0.01$ [m]: portrait graphs of (a) $\dot{\theta}$ graph in function of $dot\alpha$ and (b) θ in function of $dot\alpha$.

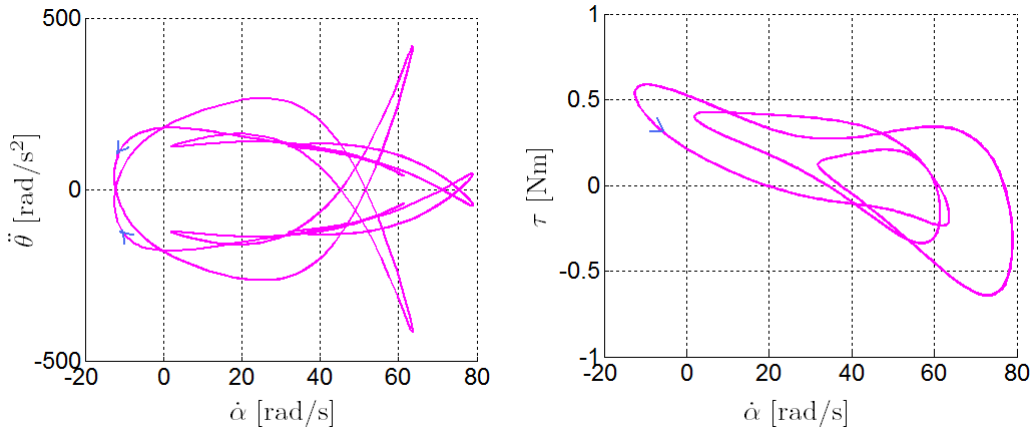

(a) (b)

Figure 22: Motor-cart-pendulum system with $d = 0.01$ [m]: portrait graphs of (a) tangent $\ddot{\theta}$ graph in function of $dot\alpha$ and (b) τ in function of $dot\alpha$.

3.5 Simulations of the motor-cart-pendulum system with friction

The differential algebraic equations to the coupled motor-cart-pendulum system with friction, Eq. (33), was integrated numerically in a range of [0.0, 25.0] seconds.

In the integration, the same parameters used in the previous simulations of the motor-cart-pendulum system without friction were adopted. That is, the same initial conditions, specifications of the motor, source voltage, and pendulum length. Also, the values used to the friction coefficients, μ_1 and μ_2, were equal to the values considered in the simulations of the motor-cart system with friction.

The values adopted to m_c, m_p and d were equal to the values used in the simulations of the motor-cart-pendulum system without frictions in the case where occurs the reversion in the relation master-slave. Thus, $m_c = 0.0$ [Kg], $m_p = 4.0$ [Kg] and $d = 0.01$ [m].

The results obtained to the angular speed of the motor and angular displacement pendulum over time are shown in Fig. 23(a) and 23(b). It is possible observe that with the consideration

of the friction, the phenomena of the reversion in the relation master-slave between the cart and the motor does not occur anymore.

Considering the frictions forces, the angular velocity of the motor shaft oscillates between 2.0 [Hz] and 10.0 [Hz] and the angular displacement of the pendulum between -43.0 [^{o}] 43.0 [^{o}]. Should be noted that this maximum angle displacement archived by the pendulum, 43.0 [^{o}], is much lower than the maximum angle in the case of non consideration of the frictions, 100.0 [^{o}] (see Fig. 19(a)). This result verifies the friction reduces the capability of the pendulum to act as a reservoir of energy.

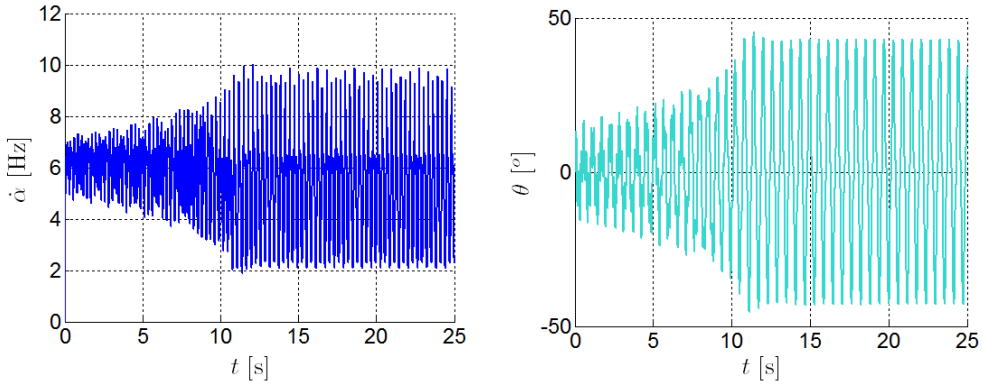

(a) (b)

Figure 23: Motor-cart-pendulum system with friction in the coupling mechanism: (a) angular velocity of the motor shaft and (b) pendulum displacement over time.

4 PROBABILISTIC MODEL

To make a stochastic analysis of the proposed systems, a system parameter is considered uncertain. It is assumed that the value of the nominal eccentricity of the pin, d is a random variable represented by the capital letter D.

The Maximum Entropy Principle (PEM) is used to construct the probability density function of this random variable, "Jaynes (1957)", "Shannon (1948)", "Sampaio and de Queiroz Lima (2012a)" and "Souza de Cursi and Sampaio (2012)", and it is assumed that the only available information is the support of D: $[d_{min}, d_{max}]$. Therefore, the Maximum Entropy Principle using Shannon entropy measure of the probability density function, p, of D, $S(p) = -\int_{d_{min}}^{d_{max}} \ln(p(d))p(d)\,dp$, yields the uniform probability density function, given by

$$p(d) = \mathbb{1}_{[d_{min},d_{max}]}(d)\,\frac{1}{d_{max}-d_{min}}\,. \tag{35}$$

where $\mathbb{1}_{[d_{min},d_{max}]}(d)$ is an indicator function that is equal to 1 for $d \in [d_{min}, d_{max}]$ and 0 otherwise.

5 NUMERICAL SIMULATIONS OF THE STOCHASTIC MOTOR-CART-PENDULUM SYSTEM WITHOUT FRICTION

As it was assumed that the value of the nominal eccentricity of the pin is a random variable, the output variables of the stochastic coupled systems are random process with parameter t. Therefore, the horizontal cart displacement is represented by the random process $\mathcal{X}$, the pendulum displacement by Θ, the angular displacement of the motor shaft by $\mathcal{A}$, the angular velocity of the motor shaft by $\dot{\mathcal{A}}$, the current by $\mathcal{C}$, the horizontal force by $\mathcal{F}$ and the torque by $\mathcal{T}$.

To make the stochastic analysis of the motor-cart-pendulum system, Monte Carlo simulations were employed to compute the mean and variance of the the random processes listed above. The support of D was assumed to be $[d_{min}, d_{max}] = [0.005,\ 0.015]$ (units in [m]).

Figure 24(a) shows one realization of Θ and, figures 24(b), 25(a) and 25(b) show the envelope graphs of $\mathcal{C}$, $\mathcal{X}$ and Θ constructed with 10^3 realizations of these random process after a convergence analysis. In each realization, the system Eq. (25), was integrated in a range of $[0.0,\ 30.0]$ seconds. The cart mass was considered to be $m_c = 1.0$ [Kg], the pendulum mass $m_p = 4.0$ [Kg], the pendulum length $l_p = 0.075$ [m], the source voltage 2.4 [Volt] and, the specifications to the motor parameters are from the motor Maxon DC brushless number 411678.

It is possible observe that the variations on the value of the nominal eccentricity of the pin bring significant dispersions to the oscillation frequencies and to the oscillation amplitude of the output variables. As shown in the deterministic analysis of the motor-cart system without friction, the FFT graphs of $\hat{x}$, $\hat{\theta}$ and $\hat{c}$ are very sensitive to variation of the parameter d. A more detailed analysis is presented in "de Queiroz Lima and Sampaio (2012b)".

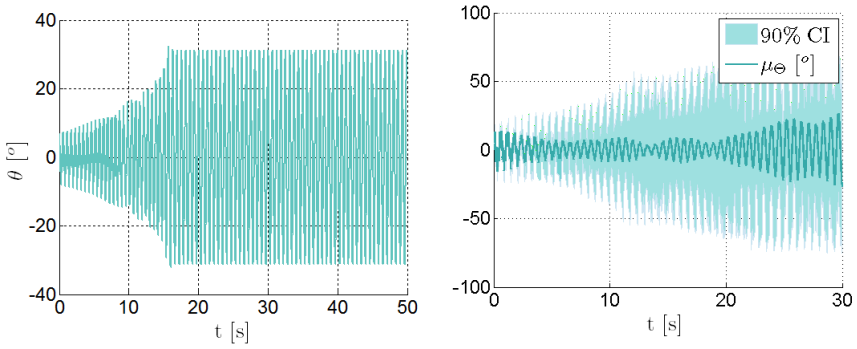

(a) (b)

Figure 24: Motor-cart-pendulum system with $d = 0.01$ [m]: (a) one realization of Θ and (b) envelope graph of Θ constructed with 10^3 realizations.

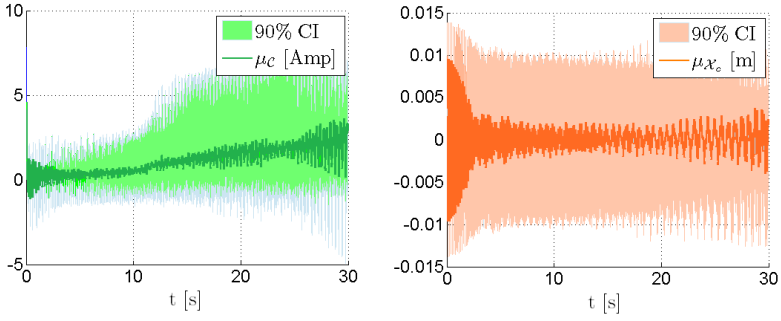

(a) (b)

Figure 25: Motor-cart-pendulum system: (a) envelope graph of $\mathcal{C}$ constructed with 10^3 realizations and (b) envelope graph of $\mathcal{X}$ constructed with 10^3 realizations.

6 CONCLUSIONS

The purpose of this paper was to analyze and compare the behavior of two electromechanical systems. The first one is composed by a cart whose motion is driven by a DC motor and in the

second one a embarked mass, a pendulum, was attached to the cart. The motor-cart system has no capacity to pump energy from the motor, it is a master-slave system: the motor drives the cart motion, the cart is driven. The only interesting feature is how the nonlinearity changes with d and m, the mass of the cart. The nonlinearity of the coupled system comes from the coupling. The motor-cart-pendulum system has a new feature, the capacity to store energy in the motion of the pendulum. With this the mechanical system can pump energy from the motor. For the motor-cart-pendulum system, for a fixed mass $m = m_c + m_p$, the relation between m_c and m_p is important. The study of the relation and how it affects the dynamics will be object of a future work. The influence of a embarked mass was demonstrated and it was shown the changes it causes in the solutions of the dynamic equations.

The nominal eccentricity of the pin of the motor, d, was characterized as a parameter that controls the nonlinearities of the equations of motion of both systems, and its influence in the dynamic equations was analyzed by the Fast Fourier Transform.

The consideration of the friction forces in the systems turned their simulations more realistic. In the case of the motor-cart-pendulum system, it was verified that the friction forces can avoid the reversion in the relation master-slave between the cart and the motor.

In the stochastic analysis, d was modeled as a random variable and the Maximum Entropy Principle was used to construct the probability model. Monte Carlo simulations were employed to compute the mean and the 90% confidence interval of the displacements of the random process that characterize the output variables of the stochastic coupled systems. It was observed that the most important effect of the variations on d were the generation of dispersions to the oscillation amplitudes and frequencies of the output variables.

As future work, a study of the distribution of mass between the cart and the pendulum in the motor-cart-pendulum system will be done. In this paper, the total mass of the motor-cart-pendulum system was considered equal to the embarked mass, a extreme case. So would be interesting to study others configurations.

7 ACKNOWLEDGMENTS

This work was supported by the Brazilian Agencies CNPQ, CAPES and Faperj.

REFERENCES

[1] Y. Rocard, *Dynamique Générale des Vibrations*, Masson et Cie., Éditeurs, Paris, France, 1943.

[2] V.O. Kononenko, *Vibrating Systems with a Limited Power Supply*, London Iliffe Books LTD, England, 1969.

[3] D. Belato, *Análise Não Linear de Sistemas Dinâmicos Holônomos Não Ideais, PhD thesis*. Department of Mechanical Engineering, Universidade Estadual de Campinas, 2002.

[4] R.R. Aguiar, *Experimental investigation and numerical analysis of the vibro-impact phenomenon, PhD thesis*. Department of Mechanical Engineering, PUC-Rio, Rio de Janeiro, Brazil, 2010.

[5] J.M. Balthazar, D.T. Mook, H.I. Weber, R.M.L.R.F. Brasil, A. Felini, D. Belato, J.L.P. Felix, An Overview on Non-Ideal Vibrations. *Meccanica*, **38**, 613–621, 2003.

[6] A.H. Nayfeh, D.T. Mook, *Nonlinear Oscillations*, John Wiley and Sons, USA, 1979.

[7] R.M. Evan-Iwanowski, *Resonance oscillations in mechanical systems*, Elsevier Publ. Co., Amsterdam, 1976.

[8] A. Fidlin, *Nonlinear Oscillations in Mechanical Engineering*, Springer, Netherlands, 2006.

[9] P. Hagedorn, *Non-linear Oscillations, 2nd Edition*, Clarendon Press, Oxford, 1988.

[10] H. Troger, A. Steindl, *Nonlinear Stability and Bifurcation Theory: An Introduction for Engineers and Applied Scientists*, Springer-Verlag, Wien, 1991.

[11] D.C. Karnopp, D.L. Margolis, R.C. Rosenberg, *System Dynamics: Modeling and Simulation of Mechatronic Systems, 4th Edition*, John Wiley and Sons, New-York, USA, 2006.

[12] W. Lacarbonara, Stuart Antman, *What is parametric excitation in Structural Dynamics? (ENOC-2008)*, Saint Petersburg, Russia, 2008.

[13] B. J. N. Persson, *Sliding Friction: Phisical Principles and Applications, 2nd Edition*, Springer-Verlag, Germany, 2000.

[14] R. Sampaio, R. de Queiroz Lima, Stochastic Analysis of an Electromechanical Coupled System with Embarked Mass. *Mecânica Computacional*, **XXXI**, 2783–2800, 2012b.

[15] R. Sampaio, R. de Queiroz Lima, Uncertainty quantification of coupled electromechanical systems with an embarked pendulum. *Diname 2013*, 2012c.

[16] E. Gourdon, N.A. Alexander, C.A. Taylor, C.H. Lamarque, S. Pernot, Nonlinear energy pumping under transient forcing with strongly nonlinear coupling: Theoretical and experimental results. *Journal of Sound and Vibration*, **300**, 522–551, 2007.

[17] E. Gourdon, *Contrôle passif de vibrations par pompage énergétique, PhD thesis*. Ecole Centrale de Lyon, France, 2006.

[18] E. Cataldo, S. Bellizzi, R. Sampaio, *Free vibrations of an uncertain energy pumping system*, Tecnical Report, PUC-Rio, 2012.

[19] E. Jaynes, Information theory and statistical mechanics. *The Physical Review*, **106**, No.4, 620-630, 1957.

[20] C.E. Shannon, A mathematical theory of communication. *Bell System Tech. J.*, **27**, 379–423 and 623–659, 1948.

[21] R. Sampaio, R. de Queiroz Lima, *Modelagem Estocástica e Geração de Amostras de Variáveis e Vetores Aleatórios*, Vol. 70, electronic address: http://www.sbmac.org.br/arquivos/notas/livro_70.pdf, Notas de Matemática Aplicada, SBMAC, 2012a.

[22] R. Sampaio, E. Souza de Cursi, *Modelagem Estocástica e Propagação de Incertezas*, Vol. 66, electronic address: http://www.sbmac.org.br/arquivos/notas/livro_66.pdf, Notas de Matemática Aplicada, SBMAC, 2012.